Gamow-Teller transition strengths from the $^{11}B(p,n)^{11}C$ reaction in the energy range 160–795 MeV

T. N. Taddeucci,[a] R. C. Byrd,[a] T. A. Carey,[a] D. E. Ciskowski,[b] C. C. Foster,[c] C. Gaarde,[d] C. D. Goodman,[c] E. Gülmez,[e] W. Huang,[c] D. J. Horen,[f] J. Larsen,[d] D. Marchlenski,[g] J. B. McClelland,[a] D. Prout,[h] J. Rapaport,[i] L. J. Rybarcyk,[a] E. Sugarbaker,[g] I. J. Van Heerden,[c],* and C. A. Whitten, Jr.[e]

[a]*Los Alamos National Laboratory, Los Alamos, New Mexico 87545*

[b]*University of Texas, Austin, Texas 78712*

[c]*Indiana University, Bloomington, Indiana 47405*

[d]*Niels Bohr Institute, Copenhagen, Denmark*

[e]*University of California, Los Angeles, California 90024*

[f]*Oak Ridge National Laboratory, Oak Ridge, Tennessee 37830*

[g]*Ohio State University, Columbus, Ohio 43210*

[h]*University of Colorado, Boulder, Colorado 80309*

[i]*Ohio University, Athens, Ohio 45701*

(Received 2 April 1990)

Zero-degree cross sections have been measured for the $^{11}B(p,n)^{11}C$ reaction at bombarding energies of $E_p = 160$, 200, 494, 644, and 795 MeV. In addition, spectra have been obtained at laboratory scattering angles of 3° and 5° at 494 MeV, and the transverse spin-flip probability at zero degrees has been measured for $E_p = 160$ MeV. These data are used to obtain estimates of the Gamow-Teller transition strength to final states in ^{11}C up to an excitation energy of $E_x \simeq 14$ MeV. The uncertainty (1 standard deviation) in the extracted transition strengths is estimated to be in the range (2–8)%. Measured cross sections for the first four excited states in ^{11}C have been compared to distorted-wave impulse approximation calculations. In this comparison, no evidence is found in the cross-section data for certain effects associated with knock-on exchange and noncentral interactions.

I. INTRODUCTION

The measured flux of electron neutrinos emitted by the Sun is apparently much smaller than that predicted by the standard-solar model.[1–3] This discrepancy can be attributed either to previously unobserved properties of the neutrino or to deficiencies in the solar model. An experimental resolution of this problem will require measuring the low-energy neutrinos from the dominant solar neutrino-production reactions or devising measurements that are sensitive to different neutrino flavors.[3–5]

Recently, ^{11}B has been proposed as a neutrino detector material that can simultaneously provide distinguishable sensitivity to the electron-neutrino flux and the flavor-inclusive neutrino flux.[6,7] The proposed technique involves detecting neutral-current flavor-inclusive excitations of states in ^{11}B and charged-current electron-neutrino transitions to the corresponding mirror states in ^{11}C. If the transition strengths for the various excitations are known, the magnitudes, as well as the ratio of the two (potentially different) neutrino fluxes, can be determined.

The charged-current transition rates (inverse β decay) are determined by the so-called Gamow-Teller ($\Delta J^\pi = 1^+$) transition strength $B(\mathrm{GT})$, for which the relevant matrix element is $\langle \sigma t^- \rangle$. The neutral-current transition strengths are determined by the matrix element $\langle \sigma t_z \rangle$ and are related to the corresponding $B(\mathrm{GT})$ by a simple numerical factor. The value of $B(\mathrm{GT})$ for the ground-state (g.s.) transition can be obtained from the measured β-decay rate of ^{11}C. The GT transition strengths for the excited states can be estimated from shell-model calculations and magnetic-dipole ($M1$) transition strengths derived from experiments.[6,7] This method is subject to large model-dependent uncertainties, however. Both isovector and isoscalar spin and current matrix elements contribute to the electromagnetic $M1$ transitions, but only the isovector spin part is relevant for neutrino excitations. A complementary and potentially better estimate of the GT transition strengths can be obtained from analysis of $^{11}B(p,n)$ cross sections.

The (p,n) reaction at intermediate energies ($E_p > 100$ MeV) has been shown to be a good probe of spin-excitation strength.[8] In particular, zero-degree (p,n) reactions are dominated by GT-type transitions. A relatively simple proportionality relationship can be applied to measured zero-degree cross sections to obtain the corresponding transition strength $B(\mathrm{GT})$.[9,10]

To date, the most detailed studies of the $^{11}B(p,n)$ reaction have been for relatively low energies. Cross-section angular distributions have been measured for $E_p = 30$ and 50 MeV by Clough *et al.*[11] and for $E_p = 16$–26 MeV by Grimes *et al.*[12] Zero-degree polarization transfer has been reported by Hiebert *et al.*[13] for $E_p = 16$–26 MeV. Recently, zero-degree cross sections were reported by Rapaport *et al.*[14] for $E_p = 492$ and 590 MeV.

In this paper we report zero-degree $^{11}B(p,n)$ cross-section measurements for bombarding energies in the range $E_p = 160$–795 MeV. In addition to these zero-degree cross sections, transverse polarization transfer at zero degrees has been measured for $E_p = 160$ MeV and cross sections for two nonzero angles have been measured for $E_p = 494$ MeV. Preliminary results based on the

analysis of a subset of these data have been privately communicated and reported in Refs. 7, 12, and 14. We present here a full analysis of the entire set of data. This analysis provides reliable estimates for the GT transition strengths to excited states in ^{11}C and also provides a quantitative test of the approximations and models used in the analysis of intermediate-energy (p,n) reactions.

II. EXPERIMENTAL METHOD AND RESULTS

Zero-degree cross sections for the ^{11}B$(p,n)^{11}$C reaction have been measured for nominal bombarding energies of 160 and 200 MeV at the Indiana University Cyclotron Facility (IUCF) and for bombarding energies of 494, 644, and 795 MeV at the Clinton P. Anderson Meson Physics Facility (LAMPF) in Los Alamos. Transverse polarization transfer was also measured with the 160-MeV beam at IUCF. A summary of experimental parameters for each measurement is presented in Table I.

The IUCF data were obtained with the beam-swinger facility[16] and six plastic (NE102) scintillation detectors with dimensions $15\times15\times102$ cm^3. The detectors were viewed at each end by RCA 4522 photomultipliers coupled by tapered Lucite light guides. Time and pulse-height signals derived from each phototube were digitized and combined in software to yield the mean arrival time, position, and total energy deposition of each neutron event. Neutron energy was determined by time of flight (TOF) with respect to a phase-stabilized cyclotron rf signal. This yields TOF modulo the beam burst period. The overall TOF resolution, independent of target contributions, was typically about 0.8 ns.

Two different detection modes were used. The 160-MeV data were obtained with the detectors configured as a six-element polarimeter.[17] In this mode the detectors form two parallel planes (three detectors per plane) perpendicular to the incident neutron flux. A neutron is required to interact once in each plane. The time and position information from each plane is then used to kinematically select $n+p$ events (which have analyzing power useful for polarimetry) from $n+$C events. This kinematic selection also resolves the beam-burst ambiguity in the TOF measurement and allows rejection of frame-overlap neutrons of lower energy. The resulting spectrum is remarkably free of background. Reconstruction of the azimuthal intensity distribution of the double-scattered neutrons allows the neutron polarization to be determined.

The 200-MeV data were obtained with the same six detectors operated in a longitudinal-singles detection mode. In this configuration the long axis of each detector is parallel to the incident neutron flux. All events that trigger only a single detector and exceed a software-selected pulse-height threshold are defined as valid. TOF to the interaction point is corrected by the measured position of each event. This technique minimizes the contribution to the resolution from the finite detector thickness and maximizes the detection efficiency for high pulse-height thresholds. Cosmic-ray events and frame-overlap neutrons are partially rejected by careful selection of the pulse-height threshold. This technique results in a somewhat poorer signal-to-noise ratio than the transverse-polarimetry detection mode, but the overall detection efficiency is much higher.

The LAMPF data were obtained with the new Neutron Time-of-Flight (NTOF) Facility.[15] The detector system consists of three liquid (BC-517S) scintillation detectors that can be configured as a neutron polarimeter.[15] Each detector is a stainless-steel tank that is subdivided into ten optically isolated cells with dimensions $10\times10\times107$ cm^3. Both ends of each cell are viewed by Amperex XP2262 phototubes coupled by tapered Lucite light guides. This detector system was operated in two different modes: transverse coincidence and transverse singles.

The physical configuration of the detector tanks is the same for both the coincidence and singles modes of operation. In singles mode, any event that triggers a sin-

TABLE I. Summary of experimental parameters for the ^{11}B$(p,n)^{11}$C measurements reported in this paper. Listed are the facility used for each measurement, the beam energy E_p, neutron flight path L, beam polarization $|p|$, beam-burst period Δt_{BB}, average beam intensity I_p, overall energy resolution δE, target areal thickness μ_t, target isotopic fraction (%), scattering angle, and detection mode. The detection modes are transverse polarimetry (TP), transverse coincidence (TC), transverse singles (TS), and longitudinal singles (LS).

Facility	IUCF	IUCF	LAMPF	LAMPF	LAMPF	LAMPF
E_p (MeV)	160	200	795	644	494	494
L (m)	45.9	132.3	617.8	617.8	617.8	341.8
$\|p\|$	0.84	0	0	0	0	0
Δt_{BB} (ns)	124.0	113.8	4968.9	4968.9	4968.9	2086.9
I_p (nA)	50	30	30	60	60	10
δE_{FWHM} (MeV)	1.3	0.73	1.25	0.68	0.66	1.0
μ_t (mg/cm^2)	146.9	110	185	185	185	185
Enrichment (%)	97.2[a]	97.2	95[b]	95	95	95
θ_{lab}	0°	0°	0°	0°	0°	0°,3°,5°
Mode	TP	LS	TC	TC	TC	TS

[a]Boron (97.2% ^{11}B, 2.8% ^{10}B).
[b]Boron (99.5% ^{11}B) plus 5% CH_2 binder.

gle tank and exceeds a software-selected threshold is considered valid.

The transverse-coincidence mode is similar to the polarimetry mode used with the IUCF detectors. The primary difference is that the azimuthal and polar scattering-angle cuts required for polarimetry are not imposed on the data. The three scintillator tanks are arranged as parallel planes perpendicular to the neutron flux. One tank serves as an analyzer plane, the remaining two tanks are spaced closely together at an average separation of 1.7 m from the front tank. Incident neutrons are required to undergo either elastic (n,n) or charge-exchange (n,p) scattering with protons in the scintillator of the front tank. Kinematic selection of these events and background rejection is accomplished in the same manner as with the IUCF detectors.

Overall TOF resolution for the LAMPF detector system, independent of target contributions, was typically better than 0.6 ns. The overall optimized time resolution was 0.45, 0.49, and 0.55 ns for 795, 644, and 494 MeV, respectively. For the 494- and 644-MeV measurements, beam time and momentum contributions to the resolution were minimized by a longitudinal focusing technique that makes use of unused accelerating cavities in the linear accelerator.[18] Time spread in the beam was minimal for the 795-MeV measurements because of decreased drift distance between the last accelerating cavity and the target. For this energy, the longitudinal focusing technique cannot be used because all accelerating cavities are in use. Momentum spread in the beam was therefore minimized by use of momentum-defining stripper foils located at dispersion points in the beam line. This technique resulted in an average beam current that was somewhat lower than that obtained at the two lower energies.

In the IUCF measurements, beam current was monitored with a split Faraday cup downstream of the target. At LAMPF, relative beam intensity was measured with secondary-emission monitors upstream of the target. Absolute normalization of the data was accomplished by comparison to ^{7}Li(p,n) yields measured under the same conditions.[19] The data presented here have been normalized to an energy-independent center-of-mass (c.m.) ^{7}Li(p,n) cross section of $\sigma(0°)=27.0\pm0.8$ mb/sr.

Zero-degree spectra of neutron yield versus excitation energy are displayed in Figs. 1 and 2. The spectra are remarkably similar over the entire range of bombarding energies. The dominant features are peaks representing the g.s., 2.0, (4.32+4.80), and (8.10+8.42) MeV levels in ^{11}C. There is also a broad complex of strength in the region from 10 to 13.8 MeV. This region includes the unresolved $T=\frac{3}{2}$ analog of the ^{11}N ground state. The peak assignments are based on the established level scheme for ^{11}C.[20]

It is assumed that the zero-degree yields in the low-excitation region ($E_x < 14$ MeV) are predominantly due to $L=0$ GT transitions. Figure 3 displays the spectra obtained at $E_p=494$ MeV for scattering angles of 3° and 5°. The spectra are plotted so that the large-GT peak at 4.5 MeV has an approximately constant amplitude. As the scattering angle increases, transitions with $L>0$ are responsible for the relative increase in yield at large-

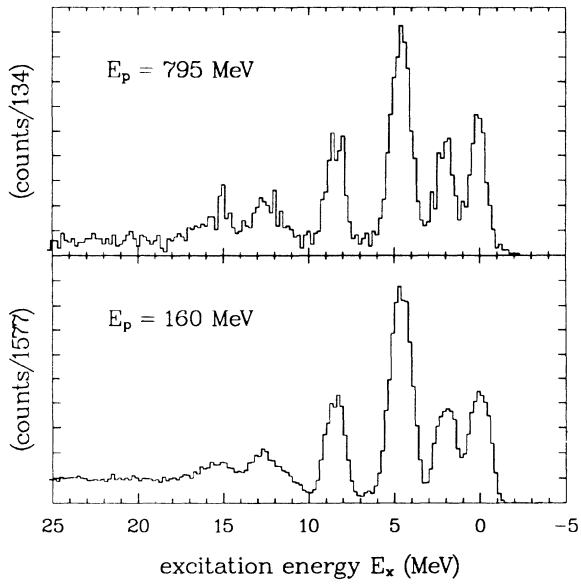

FIG. 1. Zero-degree neutron yield versus excitation energy for the ^{11}B(p,n) reaction at 160 and 795 MeV. The bin width in each spectrum is 0.2 MeV. The full-scale counts/channel is given in the vertical axis labels.

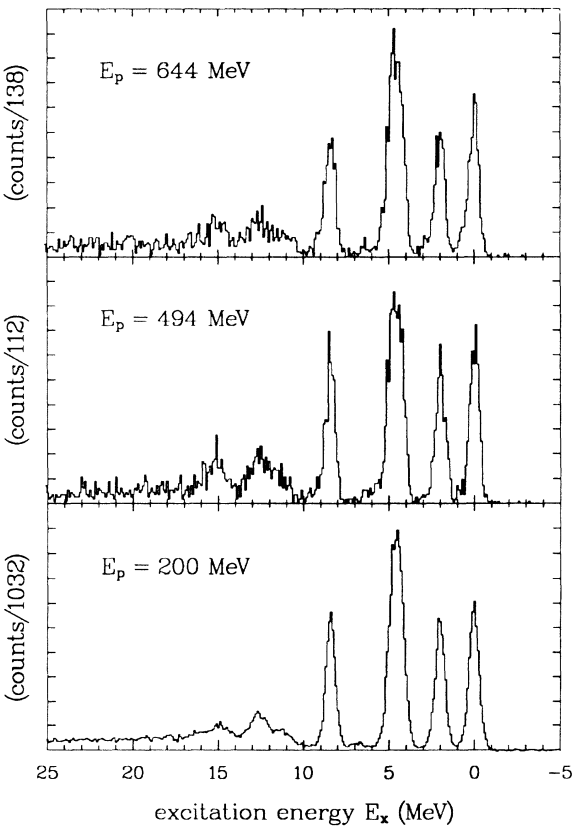

FIG. 2. Zero-degree neutron yield versus excitation energy for the ^{11}B(p,n) reaction at 200, 494, and 644 MeV. The bin width in each spectrum is 0.1 MeV. The full-scale counts/channel is given in the vertical axis labels.

excitation energies ($E_x > 10$ MeV).

Neutron yields for the distinct peaks were obtained by two methods and checked for consistency. Yields were obtained by summing between channels and also by peak fitting. A symmetric Gaussian line shape was used to fit the 160-, 200-, and 795-MeV spectra. An asymmetric Gaussian line shape with an exponential tail was used to fit the 494- and 644-MeV spectra. The more complicated line shape used for these two energies is justified by Monte Carlo simulations of the longitudinally focused beam. A modified chi-square statistic based on the Poisson distribution was used as the goodness-of-fit criterion in the fitting procedure for all energies.[21] This statistic preserves the area of the fitted peaks and gives excellent agreement with the yield determined by summing between channels.

Four peaks were simultaneously fitted in each spectrum: g.s., 2.00, 4.32, and 4.80 MeV. The relative positions were fixed by the known energy separations and the widths were constrained to be equal. The peak at $E_x \simeq 8.4$ MeV was fitted independently with an unconstrained width. The results of the fitting indicate that the 4.32- and 4.80-MeV transitions have approximately equal strength, in good agreement with shell-model estimates (see Sec. IV), but the present resolution does not allow a more quantitative estimate. The combined yield for these two transitions will be referred to as the "4.5-MeV" transition. The widths and positions obtained from fitting the peak at 8.4 MeV indicate that his peak is almost entirely due to the transition to the $\frac{5}{2}^-$ level at $E_x = 8.42$ MeV in ^{11}C. The average excitation energy was determined to be 8.47 ± 0.08 MeV. This peak will be referred to as the "8.4-MeV" transition.

The spectra in Figs. 1–3 represent raw yields and are not corrected for detector efficiency or neutron attenuation. Corrections for these effects have been made in the analysis of individual peak yields. Relative efficiency and attenuation corrections are small; for example, the corrections required for the 200-MeV data amount to a 6% increase in the yield for the 8.4-MeV transition compared to the ground state. A small amount of background yield from ^{12}C in the target is expected for the spectra obtained at LAMPF. These background events should be present as a narrow peak (see Fig. 3 in Ref. 14) at an apparent excitation energy of $E_x = 15.3$ MeV. Below this excitation energy, all of the spectra should be relatively free of background except for small contributions from the few percent of ^{10}B in the IUCF target. An estimate based on the 50-MeV ^{10,11}B(p,n) data of Clough *et al.*[11] indicates that this ^{10}B(p,n) contaminant yield is negligible at forward angles.

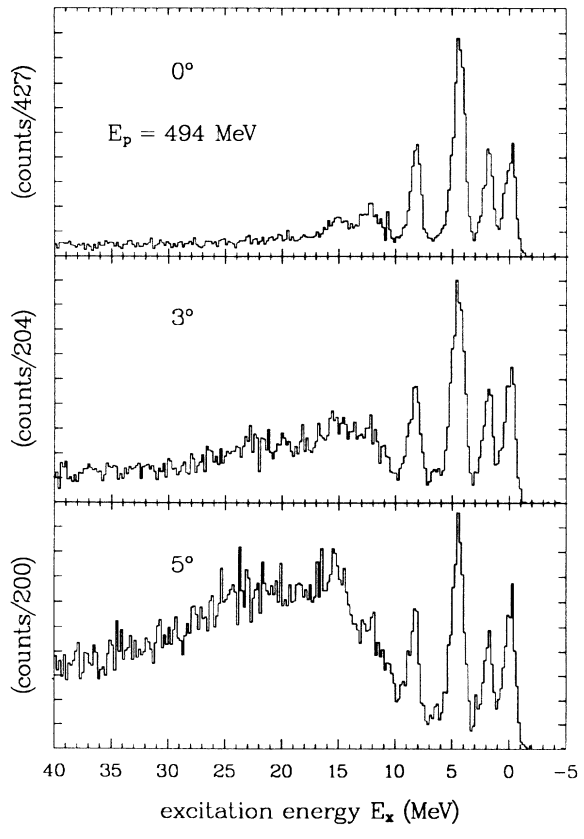

FIG. 3. Neutron yield versus excitation energy for the ^{11}B(p,n) reaction at 494 MeV and laboratory angles of 0°, 3°, and 5°. The spectra are plotted so that the peak at $E_x \simeq 4.5$ MeV has an approximately constant amplitude.

III. GAMOW-TELLER TRANSITION STRENGTH

The (p,n) cross section $\sigma_1(q,\omega)$ for low-momentum transfer $L=0$ 1^+ transitions can be related to the corresponding Gamow-Teller transition strength $B(\mathrm{GT})$ according to[10]

$$\sigma_1(q,\omega) = \hat{\sigma}_{\mathrm{GT}} F(q,\omega) B(\mathrm{GT}) , \tag{1}$$

where $\hat{\sigma}_{\mathrm{GT}}$ is a proportionality factor ("unit cross section") and $F(q,\omega)$ describes the dependence on the momentum transfer q and energy loss ω. This latter factor is defined to be unity when $(q,\omega)=0$.

The required proportionality factor for ^{11}B(p,n) can be obtained from the ground-state transition, for which the β-decay rate is known.[20] In the present analysis, we have used a ground-state transition strength $B(\mathrm{GT}) = 0.345 \pm 0.008$ obtained from the detailed study of Raman *et al.*[22] (However, see Ref. 23 and the footnote to Table IV.) The $\frac{3}{2}^- \rightarrow \frac{3}{2}^-$ ground-state (p,n) transition involves angular-momentum transfers $J^\pi = 0^+, 1^+, 2^+, 3^+$, so that

$$\sigma = \sigma_0 + \sigma_1 + \sigma_2 + \sigma_3 . \tag{2}$$

Only the 1^+ (Gamow-Teller) and 0^+ (Fermi) contributions are important at zero degrees at intermediate energies; therefore,

$$\sigma(0°) \simeq \sigma_0 + \sigma_1 . \tag{3}$$

To obtain the value of $\hat{\sigma}_{\mathrm{GT}}$ appropriate for ^{11}B(p,n) at each energy, it is necessary to know the GT fraction $f_{\mathrm{GT}} = \sigma_1/\sigma$ of the ground-state cross section, or equivalently, the ratio σ_1/σ_0. The proportionality factor is then given by

$$\hat{\sigma}_{GT}=f_{GT}\frac{\sigma(0°)}{F(q_0,\omega_0)B(GT)} . \quad (4)$$

The GT fraction can be obtained by two independent methods. The cross-section ratio σ_1/σ_0 is given by the transition strength ratio $B(GT)/B(F)$ times the ratio R^2 of GT and F unit cross sections:

$$R^2=\frac{\hat{\sigma}_{GT}}{\hat{\sigma}_F} . \quad (5)$$

In terms of this unit-cross section ratio, the GT fraction is

$$f_{GT}=\left[1+\frac{B(F)}{R^2B(GT)}\right]^{-1} , \quad (6)$$

where, for the present case, $B(F)=N-Z=1$ and $B(GT)$ is the β-decay value mentioned earlier. A systematic study of (p,n) cross sections for bombarding energies below 200 MeV has shown that R^2 is apparently a "universal" constant with no obvious nuclide dependence.[10] If this universality is assumed, then the $^{14}C(p,n)$ reaction provides the best case of resolvable pure 1^+ and 0^+ transitions from which to obtain experimental values for R^2. Cross sections for the $^{14}C(p,n)$ reaction have been measured for $E_p=160$ and 200 MeV at IUCF (Ref. 10) and for $E_p=494$, 644, and 795 MeV at LAMPF.[24] Values for the ratio R^2 obtained from these measurements are displayed in Table II. Derived values for f_{GT} are also given in this table.

An independent estimate of the GT fraction is provided by the transverse spin-flip probability $S_{NN}(0°)$. This method relies upon the observation that 1^+ transitions in the energy range 120–200 MeV have a characteristic value for the zero-degree spin-flip probability.[25] At 160 MeV, this empirical average GT spin-flip probability is $S_1=0.66\pm0.03$. The spin-flip probability S_0 for 0^+ transitions is identically zero. The ground-state transition therefore has a spin-flip probability S

$$S\sigma\simeq S_0\sigma_0+S_1\sigma_1=S_1\sigma_1 \quad (7)$$

and

$$f_{GT}=\frac{\sigma_1}{\sigma}=\frac{S}{S_1} . \quad (8)$$

Measured spin-flip probabilities for $^{11}B(p,n)$ transitions at 160 MeV are displayed in Table III. For $^{11}B(p,n)^{11}C(g.s.)$ at $E_p=160$ MeV, Eq. (6) gives $f_{GT}=0.75\pm0.01$ (Table II) and Eq. (8) gives $f_{GT}=0.77\pm0.05$. The agreement between these two independent estimates is excellent.

Proportionality factors for $^{11}B(p,n)$ at each energy have been obtained from Eq. (4) with GT fractions defined by Eq. (6). The momentum-transfer and energy-loss corrections have been estimated in the manner outlined in Ref. 10. The factor $F(q,\omega)$ typically deviates from unity by only a few percent. As an example, the largest correction is applied to the strength in the 10.0–13.8-MeV region. For $E_p=160$ MeV, we estimate that $F(q,\omega)=0.85$. As the bombarding energy increases, the momentum transfer decreases for a given excitation energy. At $E_p=494$ MeV, the correction for this same region is estimated to be $F(q,\omega)=0.96$.

TABLE II. The ratio $R^2=\hat{\sigma}_{GT}/\hat{\sigma}_F$ obtained from $^{14}C(p,n)$ measurements (Refs. 10 and 24) and the resulting Gamow-Teller fraction f_{GT} for the $^{11}B(p,n)^{11}C(g.s.)$ transition.

E_p (MeV)	R^2	f_{GT}
160	8.5±0.2	0.746±0.007
200	13.0±0.3	0.818±0.005
494	9.4±0.6	0.76±0.01
644	6.8±0.4	0.70±0.01
795	5.7±0.6	0.66±0.02

TABLE III. Measured transverse spin-flip probabilities for $^{11}B(p,n)^{11}C$ at $E_p=160$ MeV.

E_x (MeV)	$S_{NN}(0°)$
0.0	0.51±0.02
2.0	0.63±0.03
4.5	0.67±0.02
8.4	0.67±0.03
10.0–13.4	0.65±0.03

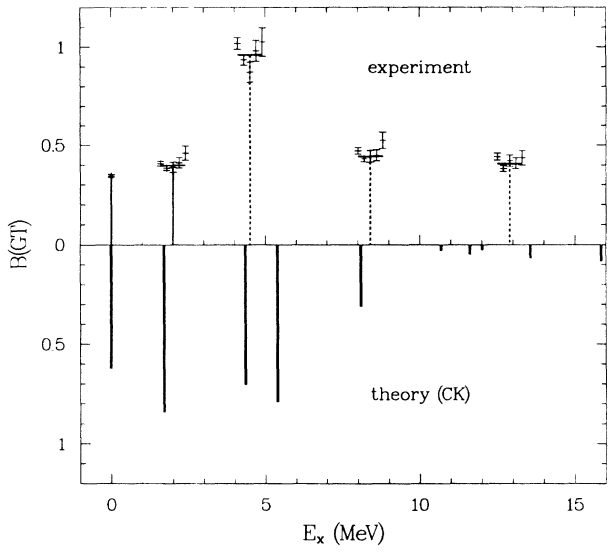

FIG. 4. Top half: Experimental Gamow-Teller transition strengths determined by comparison to the ground-state transition at five bombarding energies. The vertical lines represent the location of peaks identified in Figs. 1–3. Solid lines represent single transitions, dashed lines represent the approximate location of unresolved composite transitions. The data points for each transition are plotted with bombarding energy increasing from left to right: 160, 200, 494, 644, and 795 MeV. Weighted averages for each transition are listed in Table IV. Bottom half: Theoretical transition strengths obtained from the wave functions of Cohen and Kurath (CK) (Refs. 27, 28, and 38).

TABLE IV. Gamow-Teller transition strengths for $^{11}B(p,n)^{11}C$ transitions. The quantity δB_{avg} is the uncertainty in the weighted average of five values for each transition. The quantity δB_{std} is the standard deviation of the five values with respect to the average.

E_x (MeV)	B(GT)	δB_{avg}	δB_{std}
0.0	0.345[a]	0.008	
2.0	0.399	0.008	0.032
4.5[b]	0.961	0.017	0.060
8.4[c]	0.444	0.009	0.010
10.0–13.8	0.406	0.009	0.023

[a]Obtained from analysis in Ref. 22. The present value is based upon a ratio $g_A/g_V=-1.260\pm0.0008$ (Ref. 23) rather than the smaller value (-1.237 ± 0.008) assumed in ref. 22. Also, note that an even smaller value for this coupling-constant ratio was used in Ref. 12.

[b]Unresolved doublet, $E_x=4.32+4.80$ MeV, approximately equal strength.

[c]Unresolved doublet, $E_x=8.10+8.42$ MeV, most strength in the 8.42-MeV transition.

The transition strengths obtained at each energy by comparison to the ground-state strength are plotted in Fig. 4. The results for each transition have been averaged and tabulated in Table IV. The error bars plotted in Fig. 4 are primarily due to counting statistics. Because the GT proportionality factor is obtained from the ground-state transition and each spectrum is therefore internally calibrated, overall normalization uncertainties associated with target thickness, current integration, detector efficiency, etc., do not enter into the analysis.

Two uncertainties are given in Table IV for each transition. The first is the usual definition for the uncertainty in the weighted average,

$$(\delta B_{avg})^2=\left[\sum\frac{1}{(\delta B_i)^2}\right]^{-1}. \tag{9}$$

The second uncertainty is the standard deviation

$$(\delta B_{std})^2=\tfrac{1}{4}\sum(B_{avg}-B_i)^2, \tag{10}$$

where B_{avg} is the weighted average and the B_i are the values for each of the five bombarding energies. Energy-dependent effects associated with the effective interaction and $L>0$ contributions to the zero-degree cross sections will limit the accuracy of the proportionality formulated in Eq. (1). Such effects will introduce a nonstatistical spread in the values of B(GT) obtained by the procedure outlined above. The standard deviation defined in Eq. (10) is therefore a better indication of the true uncertainty in the transition strength obtained by application of a simple proportionality relationship. Estimates of deviations from proportionality will be discussed in the next section. It is interesting to note that the standard deviations in Table IV are in the range of 2–8 %. This range is consistent with the intrinsic accuracy of about 6% that was estimated in Ref. 10 from a systematic study of 1^+ and 0^+ transition with known transition strengths. It is also consistent with theoretical estimates discussed in Ref. 10 and in the next section.

IV. COMPARISON TO THEORY

A. Differential cross sections

In the previous section, transition strengths were obtained by applying a simple proportionality relationship to the zero-degree cross sections. Except for a smooth correction $F(q,\omega)$ for momentum transfer and energy loss, all of the (p,n) cross sections at a given bombarding energy were assumed to be related to the corresponding β-decay transition strength by the same proportionality factor $\hat{\sigma}_{GT}$. It is possible, however, that details of nuclear structure and the effective interaction will cause deviations from proportionality that will limit the ultimate accuracy of this type of analysis. In particular, contributions to the zero-degree cross sections from $L>0$ amplitudes must be considered. In this section we will attempt to assess the magnitude of these various effects with distorted-wave impulse approximation (DWIA) calculations.

Calculations have been carried out for the transitions to the first four levels in ^{11}C: $(0.00,\frac{3}{2}^-)$, $(2.00,\frac{1}{2}^-)$, $(4.32,\frac{5}{2}^-)$, and $(4.80,\frac{3}{2}^-)$. The calculations were done for nominal bombarding energies of 160, 200, 500, 650, and 800 MeV with the distorted-wave code DW81.[26] The wave functions used are those of Cohen and Kurath[27] and were obtained in the form of transition density amplitudes from the tabulation of Lee and Kurath.[28] The $J(LS)=1(01)$ amplitudes were renormalized by the factor $(B_{expt}/B_{thy})^{1/2}$ to give the experimentally determined values of B(GT) listed in Table IV. Because the 4.32- and 4.80-MeV transitions were not resolved experimentally, the 1(01) amplitudes for these transitions were normalized by the same factor to give the summed B(GT) of Table IV. Radial form factors were calculated with harmonic-oscillator wave functions with an effective oscillator parameter of $b=1.50$ fm^{-1}.[12] Optical-potential parameters were obtained from the ^{12}C potentials (DWS+MSO) of Meyer *et al.*[29] for $E_p=160$ and 200 MeV, Blanpied *et al.*[30] for 800 MeV, and the 398- and 698-MeV parameters of Jones *et al.*[31] were used for the 500- and 650-MeV calculations, respectively. The effective interaction was obtained from the t-matrix parametrizations of Franey and Love[32] for $E_p=175$, 210, 515, 650, and 800 MeV.

Several different normalization factors have been applied to the calculated cross sections. As discussed by Grimes *et al.* in Ref. 12, use of an oscillator parameter obtained from fitting electron scattering data requires an approximate correction to the cross section of the form $\sigma\rightarrow(A/A-1)^L\sigma$, where $L=0$ is used for 0^+ and 1^+ cross sections, and $L=2$ is used for 2^+ and 3^+. Grimes *et al.* also applied an isovector quadrupole renormalization factor of 0.5 to the $J^\pi=2^+$ cross sections in their analysis. For simplicity, we have not applied this factor in the present analysis, and its omission does not measurably affect our conclusions. Normalization factors for

TABLE V. DWIA normalization factors for ^{11}B(p,n) transitions. The summed cross section for each transition is given by $\sigma = N_0\sigma_0 + N_1\sigma_1 + N_2\sigma_2 + N_3\sigma_3$. At each bombarding energy, N_0 for the 4.80-MeV transition is taken to be the same as for the ground state. The last column, labeled $N_0(C)$, gives the 0^+ normalization factor when only the central (C) interaction is used in the calculations.

E_p (MeV)	E_x (MeV)	N_0	N_1	N_2	N_3	$N_0(C)$
160	0.00	0.98	1.0	1.21	1.21	0.84
200	0.00	0.86	1.0	1.21	1.21	0.73
500	0.00	0.54	1.0	1.21	1.21	0.52
650	0.00	0.48	1.0	1.21	1.21	0.46
800	0.00	0.40	1.0	1.21	1.21	0.37
	2.00		1.0	1.21		
	4.32		1.0	1.21	1.21	
	4.80	0.40	1.0	1.21	1.21	

the $J^\pi = 0^+$ cross sections are obtained from the ratio

$$N_0 = \frac{(\sigma_1/\sigma_0)_{\text{DWIA}}}{(\sigma_1/\sigma_0)_{\text{expt}}} \tag{11}$$

for ^{14}C(p,n) transitions to the 2.31-MeV (0^+) and 3.95-MeV (1^+) states in ^{14}N. These calculations were performed in the same manner as outlined above, with the 1(01) amplitude for the 3.95-MeV transition normalized to reproduce the experimental GT transition strength.[10] The factor N_0 can be thought of as supplying a necessary renormalization of the V_τ piece of the effective interaction, which is difficult to calculate because of density dependence.[33] All of the DWIA normalization factors used in the present analysis are given in Table V.

Measured zero-degree cross sections for the ^{11}B(p,n) ground-state transition are plotted in Fig. 5. The solid line in this figure represents the calculated cross section with all normalization factors applied. There will be some energy dependence of this cross section due to the energy dependence of the ratio σ_1/σ_0. This dependence seems to be well reproduced between 160 and 200 MeV.

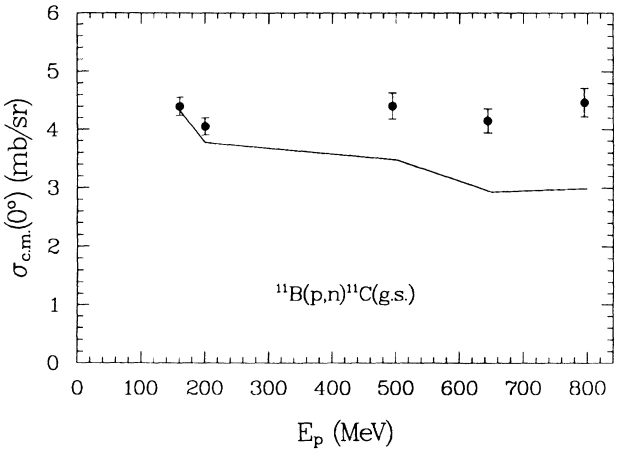

FIG. 5. Zero-degree cross section versus bombarding energy for the ^{11}B(p,n)^{11}C(g.s.) transition. The solid line represents the full DWIA calculations discussed in the text.

The empirical optical potentials used here for 500–800 MeV may not be the best possible choice and were selected merely for convenience; the underprediction of the cross sections for these higher energies is therefore probably not too significant. It is important to recognize that all information about excited-state transition strengths, which is the main point of this paper, is derived from relative cross sections with respect to the ground state. Additional effort toward improving the absolute agreement between the measured and calculated cross-section magnitudes is therefore not warranted in the present study.

Calculated angular distributions for 500-MeV ^{11}B(p,n) transitions to the ground state, 2.0-MeV, and (4.32+4.80)-MeV states in ^{11}C are displayed in Figs. 6–8. The immediate conclusion to be drawn from these calcu-

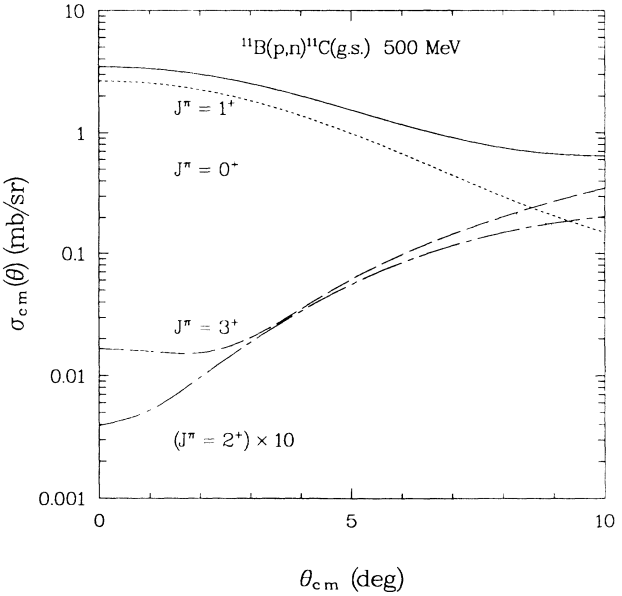

FIG. 6. Calculated angular distribution for the ^{11}B(p,n)^{11}C(g.s.) reaction at $E_p = 500$ MeV. The solid line represents the sum of all possible angular-momentum transfers: 0^+ (dotted), 1^+ (dashed), 2^+ (chain-dashed), and 3^+ (chain-dotted). The plotted distributions include the normalization factors of Table V.

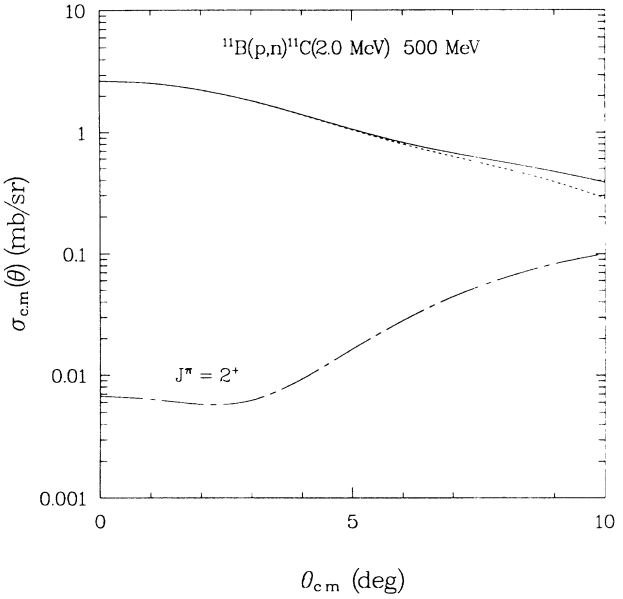

FIG. 7. Calculated angular distribution for the ^{11}B$(p,n)^{11}$C(2.0 MeV) reaction at $E_p = 500$ MeV. The solid line represents the sum of all possible angular-momentum transfers: 1^+ (dashed) and 2^+ (chain-dashed). The plotted distributions include the normalization factors of Table V.

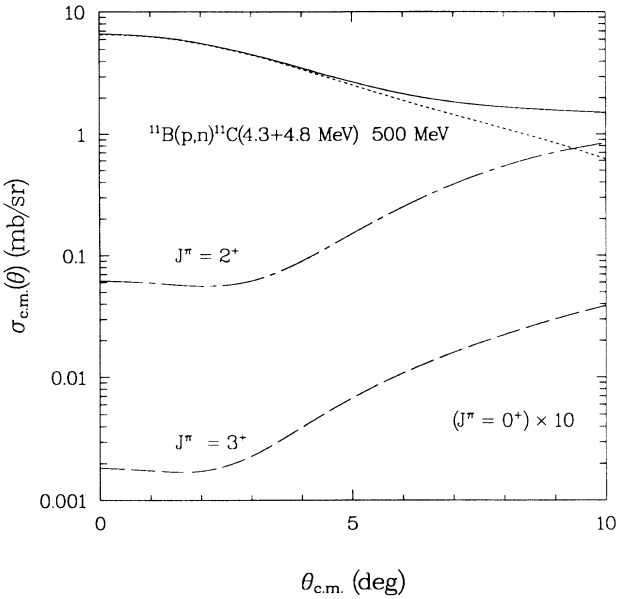

FIG. 8. Calculated angular distribution for the ^{11}B$(p,n)^{11}$C(4.32+4.80 MeV) reaction at $E_p = 500$ MeV. The solid line represents the sum of all possible angular-momentum transfers: 0^+ (dotted), 1^+ (dashed), 2^+ (chain-dashed), and 3^+ (chain-dotted). The plotted distributions include the normalization factors of Table V.

lations is that only the $J^\pi = 0^+, 1^+$ (Fermi and Gamow-Teller) cross sections are important at zero degrees, and the $J^\pi = 2^+, 3^+$ cross sections become significant only beyond about 6° ($q_{c.m.} \simeq 0.5$ fm^{-1}). These predictions can be tested, to a limited extent, by the non-zero-degree data obtained for $E_p = 494$ MeV.

In Fig. 9 we plot experimental and calculated cross-section ratios as a function of scattering angle. Two ratios are plotted: $\sigma(2.0)/\sigma(\text{g.s.})$ and $\sigma(2.0)/\sigma(4.5)$. The measured ratio involving the ground state becomes smaller with angle, while the measured ratio for the two excited states is essentially constant. If the $J^\pi = 2^+, 3^+$ cross sections are negligible at small angles, then the experimental ratios have a simple explanation. At small angles, the cross-section distribution for an $L = 0$ transition will have the approximate dependence[10]

$$\sigma(q) \simeq \sigma(0) \exp\left[-q^2 \frac{\langle r^2 \rangle}{3}\right], \tag{12}$$

where the factor $\langle r^2 \rangle$ is primarily the sum of the mean-square radius of the transition density and the effective interaction. The 2.0- and 4.5-MeV transitions are both 1^+ transitions driven by the central $V_{\sigma\tau}$ term of the effective interaction. The value of $\langle r^2 \rangle$ will be very nearly the same for these transitions and therefore the cross-section ratio as a function of momentum transfer (or scattering angle) will be constant. The ground-state transition is a sum of Gamow-Teller and Fermi transitions. The V_τ interaction is of shorter range than $V_{\sigma\tau}$ and has a smaller mean-square radius. The 0^+ cross-section distribution will therefore decrease less rapidly with momentum transfer than the 1^+ distribution. In the ratio $\sigma(2.0)/\sigma(\text{g.s.})$, the value of $\sigma(\text{g.s.})$ will therefore decrease less rapidly than $\sigma(2.0)$ and the ratio will become smaller as the scattering angle increases.

A more quantitative estimate of the angular dependence of the cross-section ratios is provided by DWIA calculations. In Fig. 9, calculated ratios are presented for three different conditions. The solid lines correspond to calculations employing the full interaction (central, spin

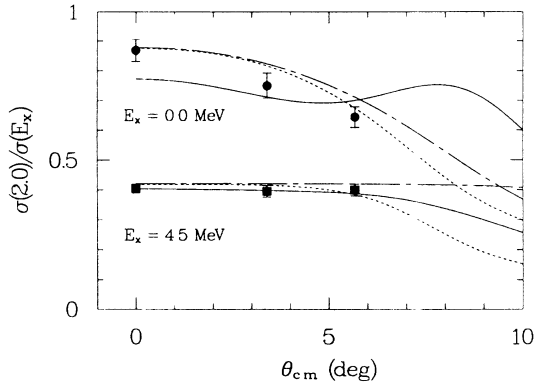

FIG. 9. Cross-section ratios versus scattering angle for $E_p = 494$ MeV. The two ratios are $\sigma(2.0)/\sigma(\text{g.s.})$ (circles) and $\sigma(2.0)/\sigma(4.5)$ (squares). The solid lines represent DWIA calculations employing the full effective interaction and all allowed angular-momentum transfers. The dashed lines represent calculations in which only a central interaction was used for $J^\pi = 0^+, 1^+$. The chain-dashed lines represent calculations for $J^\pi = 0^+, 1^+$ only and a central interaction only.

orbit, tensor) and contributions from all angular-momentum transfers ($J^\pi=0^+,1^+,2^+,3^+$). The dashed lines correspond to calculations in which only the central interaction is included for $J^\pi=0^+,1^+$, but the full interaction is used for $J^\pi=2^+,3^+$. The chain-dashed lines correspond to calculations for a central interaction only and $J^\pi=0^+,1^+$ only.

Over the measured range, all three calculations do a reasonable job of reproducing the ratio $\sigma(2.0)/\sigma(4.5)$. This supports the idea that these transitions are insensitive to the noncentral interaction and $L>0$ amplitudes at small angles. However, the ratio involving the ground state is reproduced only when the noncentral interaction terms are omitted from the calculations for $J^\pi=0^+,1^+$. Inclusion of the $J^\pi=2^+,3^+$ contributions only makes a small improvement in the calculated ratio for angles larger than about 5°. The $\sigma(2.0)/\sigma(\text{g.s.})$ ratio therefore appears to be a sensitive test for the effect of noncentral terms in the interaction.

The ground-state transition is affected by the noncentral interaction terms in two different ways. The 0^+ cross section is *decreased* by an interference originating with the microscopic spin-orbit and optical-spin-orbit potentials.[33] The tensor interaction has a similar but smaller effect. The net effect on the cross section is largest at low energies (0.90 at 160 MeV) and becomes insignificant for energies greater than about 450 MeV. The 1^+ cross section is affected in the opposite manner by the tensor-exchange amplitude. In the present calculations for $E_p \geq 500$ MeV, the tensor interaction significantly *increases* the 1^+ g.s. cross section (1.29 at 800 MeV). A similar but smaller (1.15 at 800 MeV) effect is predicted for the 4.32-MeV transition.

The measured cross-section-ratio angular distributions do not support the predicted effects of noncentral interactions on the 0^+ and 1^+ cross sections. Ratios of zero-degree cross sections also show no evidence for these effects. Experimental and calculated ratios of zero-degree cross sections are displayed in Fig. 10. The calculated ratios are full interaction, $J^\pi=0^+,1^+,2^+,3^+$ (solid line) and central interaction only, $J^\pi=0^+,1^+$ only (dashed line). As previously noted, the $J^\pi=2^+,3^+$ cross sections make a negligible contribution to the zero-degree ratios. The sole exception to this is the $J^\pi=2^+$ cross section for the 4.32-MeV transition. This cross section contributes 2.7 and 3.6% of the calculated 4.32+4.80 zero-degree cross section at 650 and 800 MeV, respectively. The comparisons in Fig. 10 lead to the same conclusion as those in Fig. 9: the best description of the cross-section data is obtained when the noncentral interaction is omitted from the $J^\pi=0^+,1^+$ calculations.

B. Polarization transfer

Additional information about the noncentral interaction can be obtained from spin observables. The tensor component in particular is predicted to have a large energy-dependent effect on polarization-transfer observables. In Fig. 11 we plot the calculated transverse-polarization transfer coefficient $D_{NN}(0°)$ ($D_{NN}=1-2S_{NN}$) for the g.s. and 2.0-MeV 1^+ transitions. In the 160–200-MeV energy range the calculated values for $D_{NN}(0°)$ agree quite well with the empirical average of -0.33 ± 0.05 for 1^+ transitions.[25] As the bombarding energy increases, however, the calculations employing the full interaction ($C+LS+T$) tend toward zero. Note that the calculated values for the polarization transfer are essentially the same for the two transitions. This contrasts strongly with the differential cross sections, which show much different sensitivities to the tensor interaction (Figs. 9 and 10).

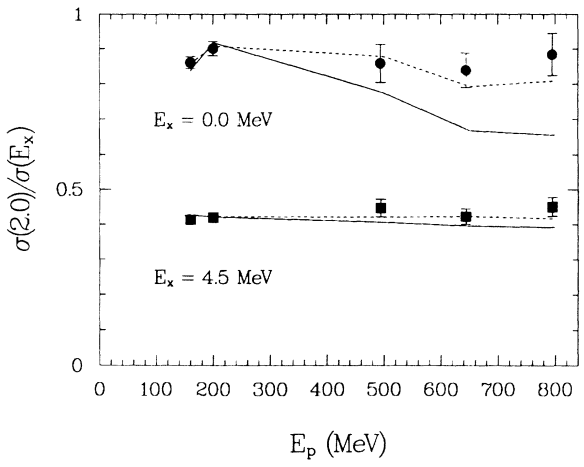

FIG. 10. Zero-degree cross-section ratios versus bombarding energy. The two ratios are $\sigma(2.0)/\sigma(\text{g.s.})$ (circles) and $\sigma(2.0)/\sigma(4.5)$ (squares). The solid lines represent DWIA calculations employing the full effective interaction and all allowed angular-momentum transfers. The dashed lines represent calculations for $J^\pi=0^+,1^+$ only and a central interaction only.

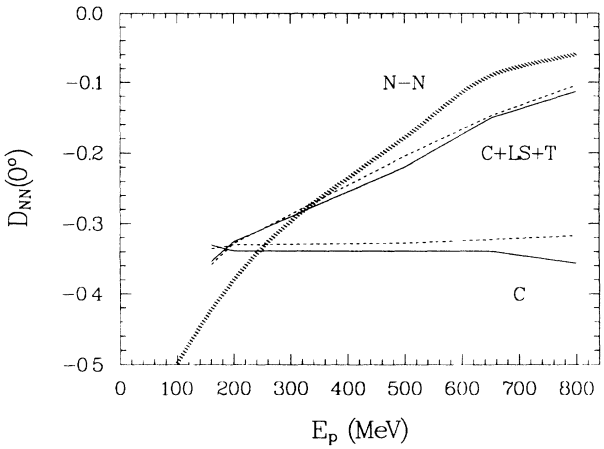

FIG. 11. Calculated values for the transverse-polarization transfer coefficient $D_{NN}(0°)$. The solid lines correspond to the $^{11}B(p,n)^{11}C(\text{g.s.})$ transition, the dashed lines correspond to the 2.0-MeV transition. Results are shown for calculations employing the central interaction (C) only, and for calculations employing the full interaction ($C+LS+T$). The thick-hashed line corresponds to an $L=0$ $J^\pi=1^+$ planes-wave estimate based on free NN scattering amplitudes.

The polarization-transfer predictions contrast with the cross sections in another way as well: there is some positive experimental evidence for the tensor-interaction effects. This evidence comes from the ^{6}Li(p,n) reaction, which is dominated by the $1^+ \rightarrow 0^+$ g.s. transition at 0°.[34] The experimental value for the transverse-polarization transfer coefficient for this reaction is $D_{NN}(0°) = -0.33 \pm 0.02$ at 200 MeV.[25,34] At 800 MeV, McNaughton, Spinka, and Shimizu[35] find that $D_{NN}(0°) = -0.03 \pm 0.06$, in good agreement with the trend displayed in Fig. 11.

The energy dependence of $D_{NN}(0°)$ can be easily understood in terms of the free nucleon-nucleon (NN) amplitudes. If the isovector NN scattering amplitude is represented in the form

$$M(q) = A + C(\sigma_1 + \sigma_2)\cdot\hat{\mathbf{n}} + \tfrac{1}{3}(B+E+F)\sigma_1\cdot\sigma_2 + \tfrac{1}{3}(E-B)S_{12}(\hat{\mathbf{q}}) + \tfrac{1}{3}(F-B)S_{12}(\hat{\mathbf{p}}) , \quad (13)$$

where

$$\mathbf{q} = \mathbf{k}_i - \mathbf{k}_f ,$$
$$\mathbf{n} = \mathbf{k}_i \times \mathbf{k}_f , \quad (14)$$

and

$$\hat{\mathbf{p}} = \hat{\mathbf{n}} \times \hat{\mathbf{q}} ,$$

then, in the context of the plane-waves impulse approximation, it is straightforward to show[36] that, for $L=0$, 1^+ transitions at 0° (where $C=0$, $E=B$), the transverse-polarization transfer coefficient can be expressed as

$$D_{NN} = \frac{-F^2}{F^2+2B^2} . \quad (15)$$

If the coefficient of the tensor operator $S_{12}(\hat{\mathbf{p}})$ is zero ($F=B$), then $D_{NN} = -\frac{1}{3}$. If this coefficient is not zero, then D_{NN} will differ from $-\frac{1}{3}$. Values for the NN amplitudes in Eq. (15) have been obtained from the phase-shift solution of Arndt and Roper.[37] The resultant prediction for D_{NN} is plotted as the thick-hashed line in Fig. 11. Good qualitative correspondence is observed between this prediction based on free NN amplitudes, the DWIA calculations, and the ^{6}Li(p,n) measurements discussed earlier.

From the consideration of both differential cross sections and zero-degree polarization transfer, we are left with two seemingly contradictory conclusions: the differential cross sections are best described by omitting the spin-orbit and tensor interactions, while polarization-transfer measurements are best explained by including the tensor interaction. This problem may originate in the formulation of the effective t-matrix interaction: the local coordinate-space representation used by Franey and Love has no term directly analogous to the $S_{12}(\hat{\mathbf{p}})$ operator in the NN scattering matrix. Instead, the knock-on exchange amplitude associated with the $S_{12}(\hat{\mathbf{r}})$ operator plays this role. An alternate formulation for the effective tensor interaction may be required to obtain consistency between the cross-section and polarization-transfer results. Additional measurements of polarization transfer in the energy range 200–800 MeV would probably be of great value in helping to define this component of the interaction.

C. Gamow-Teller strength

In Fig. 4, the theoretical transition strengths obtained from the Cohen and Kurath wave functions[27,28,38] are compared to the experimental results. The relative distribution of strength for the first four levels is qualitatively the same. The normalization factors (experiment/theory) are 0.55, 0.47, and 0.64 for the g.s., 2.0-MeV, and (4.32+4.80)-MeV transitions, respectively. For the higher-lying states, the ratio of experiment to theory is much different. The experimental strength in the 8.4-MeV transition is 1.43 times larger than theory, and the region from 10 to 13.8 MeV has approximately 1.58 times as much strength as the theoretical prediction for the 10–15-MeV region. This latter factor would be even larger if the additional experimental strength observed in the broad "peak" near $E_x \simeq 15$ MeV could be included. In terms of the overall distribution of strength, the Cohen and Kurath wave functions are thus seen to put too much strength in the lower-lying levels and not enough at higher excitations. This incorrect distribution of strength probably indicates the need for extending the shell-model configuration space.

The theoretical levels depicted in Fig. 4 account for 97.2% of the total calculated β^- strength[38] of $\sum B(\mathrm{GT})_{\mathrm{thy}} = 3.628$. The total experimental strength, summed over the region from 0 to 13.8 MeV, is $\sum B(\mathrm{GT})_{\mathrm{expt}} = 2.56 \pm 0.07$, or 71% of the theoretical value. This percentage is consistent with that reported in Ref. 12 by Grimes *et al.* As noted earlier, some additional experimental GT strength is evident in the region near $E_x \simeq 15$ MeV, presumably due to $T = \frac{3}{2}$ excitations. Because of concerns about ^{12}C(p,n) background and $L>0$ contributions, we have not attempted to extract GT transition strength for this region. Additional measurements of cross-section angular distributions with higher resolution could potentially provide more quantitative information about this region.

V. SUMMARY AND CONCLUSIONS

Zero-degree sections have been measured for the ^{11}B(p,n) reaction at 160, 200, 494, 644, and 795 MeV. Gamow-Teller transition strengths for transitions to excited states in ^{11}C have been obtained by comparison to the g.s. transition, for which the β-decay rate is known. This procedure internally calibrates each spectrum and eliminates contributions from absolute normalization errors. The main source of systematic error in the extracted transition strengths comes from the decomposition of the zero-degree ground-state cross section into its 1^+ and 0^+ components. The 1^+ fraction of the ground-state cross section can be inferred from measured ratios of pure 1^+ and 0^+ transitions in ^{14}C(p,n), or obtained from the zero-degree spin-flip probability. These two independent methods are compared for $E_p = 160$ MeV and excellent agreement is obtained.

The proportionality between zero-degree (p,n) cross sections and GT transition strengths can be affected by $L>0$ contributions and by structure and energy-dependent effects associated with the noncentral terms of the effective interaction. DWIA calculations indicate that contributions from $J^{\pi}=2^{+},3^{+}$ are negligible at zero degrees. The same calculations predict substantial deviations from proportionality for the g.s. $J^{\pi}=0^{+},1^{+}$ and 4.32-MeV $J^{\pi}=1^{+}$ transitions. However, comparison of measured and calculated cross-section ratios reveals no evidence for the predicted nonproportionality. In fact, the best agreement between experiment and theory is obtained when the noncentral terms are omitted from the DWIA calculations.

The wide energy range spanned by the present data provides an excellent measure of the absolute uncertainty implicit in the assumed proportionality between (p,n) cross sections and β-decay transition strengths. We find that estimated transition strengths have a 1-standard-deviation spread in values in the range of 2–8 %. This spread is very consistent with the uncertainty of about 6% observed in a systematic survey of lower-energy data.[10] It is unlikely that the present uncertainties will be reduced until a better understanding is obtained of the role that noncentral interactions and exchange amplitudes play in low-momentum-transfer transitions. It is important to emphasize, however, that the present results are firmly grounded in empirical systematics and are therefore largely independent of the success or failure that DWIA reaction models have in describing details of the data.

ACKNOWLEDGMENTS

We would like to acknowledge the assistance of Professor W. P. Alford, R. Alarcon, D. Krofcheck, D. Mercer, W. S. Sailor, T. P. Welch, and D. Wang with various aspects of the data acquisition. This work was supported in part by the U.S. Department of Energy (under contract with the University of California and Martin Marietta Energy Systems, Inc.), the National Science Foundation, and the Danish Natural Science Research Council.

*Permanent address: University of the Western Cape, Private Bag X17, Bellville 7530, South Africa.

[1]Raymond Davis, Jr., Don S. Harmer, and Kenneth C. Hoffman, Phys. Rev. Lett. **20**, 1205 (1968); J. K. Rowley, B. T. Cleveland, and R. Davis, Jr., in *Solar Neutrinos and Neutrino Astronomy (Lead High School, Lead, South Dakota)*, Proceedings of a Conference on Solar Neutrinos and Neutrino Astronomy, sponsored by Homestake Mining Company, AIP Conf. Proc. No. 126, edited by M. L. Cherry, K. Lande, and W. A. Fowler (AIP, New York, 1984), pp. 1–21.

[2]K. S. Hirata, T. Kajita, K. Kifune, K. Kihara, M. Nakahata, K. Nakamura, S. Ohara, Y. Oyama, N. Sato, M. Takita, Y. Totsuka, Y. Yaginuma, M. Mori, A. Suzuki, K. Takahashi, T. Tanimori, M. Yamada, M. Koshiba, T. Suda, K. Miyano, H. Miyata, H. Takei, K. Kaneyuki, Y. Nagashima, Y. Suzuki, E. W. Beier, L. R. Feldscher, E. D. Frank, W. Frati, S. B. Kim, A. K. Mann, F. M. Newcomer, R. Van Berg, and W. Zhang, Phys. Rev. Lett. **63**, 16 (1989).

[3]John N. Bahcall and Roger K. Ulrich, Rev. Mod. Phys. **60**, 297 (1988).

[4]Joseph Weneser and Gerhart Friedlander, Science **235**, 755 (1987).

[5]Gerhart Friedlander and Joseph Weneser, Science **235**, 760 (1987).

[6]R. S. Raghavan, Sandip Pakvasa, and B. A. Brown, Phys. Rev. Lett. **57**, 1801 (1986).

[7]R. S. Raghavan and Sandip Pakvasa, Phys. Rev. D **37**, 849 (1988).

[8]C. Gaarde, J. Rapaport, T. N. Taddeucci, C. D. Goodman, C. C. Foster, D. E. Bainum, C. A. Goulding, M. B. Greenfield, D. J. Horen, and E. Sugarbaker, Nucl. Phys. **A369**, 258 (1981).

[9]C. D. Goodman, C. A. Goulding, M. B. Greenfield, J. Rapaport, D. E. Bainum, C. C. Foster, W. G. Love, and F. Petrovich, Phys. Rev. Lett. **44**, 1755 (1980).

[10]T. N. Taddeucci, C. A. Goulding, T. A. Carey, R. C. Byrd, C. D. Goodman, G. Gaarde, J. Larsen, D. Horen, J. Rapaport, and E. Sugarbaker, Nucl. Phys. **A469**, 125 (1987).

[11]A. S. Clough, C. J. Batty, B. E. Bonner, and L. E. Williams, Nucl. Phys. **A143**, 385 (1970).

[12]S. M. Grimes, J. D. Anderson, J. C. Davis, R. H. Howell, C. Wong, A. W. Carpenter, J. A. Carr, and F. Petrovich, Phys. Rev. C **31**, 1679 (1985).

[13]J. C. Hiebert, R. G. Graves, L. C. Northcliffe, R. L. York, E. P. Chamberlin, and J. M. Moss, Phys. Rev. Lett. **37**, 276 (1976).

[14]J. Rapaport, P. W. Lisowski, J. L. Ullmann, R. C. Byrd, T. A. Carey, J. B. McClelland, L. J. Rybarcyk, T. N. Taddeucci, R. C. Haight, N. S. P. King, G. L. Morgan, D. A. Clark, D. E. Ciskowski, D. A. Lind, R. Smythe, C. D. Zafiratos, D. Prout, E. R. Sugarbaker, D. Marchlenski, W. P. Alford, and W. G. Love, Phys. Rev. C **39**, 1929 (1989).

[15]J. B. McClelland, Can. J. Phys. **65**, 633 (1987); in *Spin Observables of Nuclear Probes*, Proceedings of the Telluride International Conference on Spin Observables of Nuclear Probes, 1988, Telluride, Colorado, edited by Charles J. Horowitz, Charles D. Goodman, and George E. Walker (Plenum, New York, 1988), p. 183.

[16]C. D. Goodman, J. Rapaport, D. E. Bainum, and C. E. Brient, Nucl. Instrum. Methods **151**, 125 (1978); C. D. Goodman, J. Rapaport, D. E. Bainum, M. B. Greenfield, and C. A. Goulding, IEEE Trans. Nucl. Sci. **25**, 577 (1978).

[17]T. N. Taddeucci, C. D. Goodman, R. C. Byrd, T. A. Carey, D. J. Horen, J. Rapaport, and E. Sugarbaker, Nucl. Instrum. Methods A **241**, 448 (1985).

[18]J. B. McClelland, D. A. Clark, J. L. Davis, R. C. Haight, R. W. Johnson, N. S. P. King, G. L. Morgan, L. J. Rybarcyk, J. Ullmann, P. Lisowski, W. R. Smythe, D. A. Lind, C. D. Zafiratos, and J. Rapaport, Nucl. Instrum. Methods A **276**, 35 (1989).

[19]T. N. Taddeucci, W. P. Alford, M. Barlett, R. C. Byrd, T. A. Carey, D. E. Ciskowski, C. C. Foster, C. Gaarde, C. D. Goodman, C. A. Goulding, E. Gülmez, W. Huang, D. J. Horen, J. Larsen, D. Marchlenski, J. B. McClelland, D. Prout, J. Rapaport, L. J. Rybarcyk, W. C. Sailor, E. Sugarbaker, and C. A. Whitten, Jr., Phys. Rev. C **41**, 2548 (1990).

[20]F. Ajzenberg-Selove, Nucl. Phys. **A433**, 1 (1985).
[21]Steve Baker and Robert D. Cousins, Nucl. Instrum. Methods **221**, 437 (1984).
[22]S. Raman, C. A. Houser, T. A. Walkiewicz, and I. S. Towner, Atomic Data Nucl. Data Tables **21**, 567 (1978).
[23]D. H. Wilkinson, Nucl. Phys. **A377**, 474 (1982).
[24]E. Sugarbaker, D. Marchlenski, T. N. Taddeucci, L. J. Rybarcyk, J. B. McClelland, T. A. Carey, R. C. Byrd, C. D. Goodman, W. Huang, J. Rapaport. D. Mercer, D. Prout, W. P. Alford, E. Gülmez, C. A. Whitten, Jr., and D. Ciskowski, Phys. Rev. Lett. **65**, 551 (1990).
[25]T. N. Taddeucci, Can. J. Phys. **65**, 557 (1987).
[26]Program DWBA70, R. Schaeffer and J. Raynal (unpublished); extended version DW81 by J. R. Comfort (unpublished).
[27]S. Cohen and D. Kurath, Nucl. Phys. **73**, 1 (1965).
[28]T.-S.H. Lee and D. Kurath, Phys. Rev. C **21**, 293 (1980).
[29]H. O. Meyer, P. Schwandt, W. W. Jacobs, and J. R. Hall, Phys. Rev. C **27**, 459 (1983).
[30]G. S. Blanpied, B. G. Ritchie, M. L. Barlett, G. W. Hoffmann, J. A. McGill, M. A. Franey, and M. Gazzaly, Phys. Rev. C **32**, 2152 (1985).
[31]K. W. Jones, C. Glashausser, R. de Swiniarski, S. Nanda, T. A. Carey, W. Cornelius, J. M. Moss, J. B. McClelland, J. R. Comfort, J.-L. Escudie, M. Gazzaly, N. Hintz, G. Igo, M. Haji-Saeid, and C. A. Whitten, Jr., Phys. Rev. C **33**, 17 (1986).
[32]M. A. Franey and W. G. Love, Phys. Rev. C **31**, 488 (1985).
[33]W. G. Love, K. Nakayama, and M. A. Franey, Phys. Rev. Lett. **59**, 1401 (1987).
[34]J. Rapaport, C. C. Foster, C. D. Goodman, C. A. Goulding, T. N. Taddeucci, D. J. Horen, E. R. Sugarbaker, C. Gaarde, J. Larsen, J. A. Carr, F. Petrovich, and M. J. Threapleton, Phys. Rev. C **41**, 1920 (1990).
[35]M. W. McNaughton, H. Spinka, and H. Shimizu, Nucl. Instrum. Methods A **243**, 137 (1986).
[36]J. M. Moss, Phys. Rev. C **26**, 727 (1982).
[37]R. A. Arndt and L. D. Roper, Scattering Analyses Interactive Dial-in (SAID) program, phase-shift solution SM88, Virginia Polytechnic Institute and State University (unpublished).
[38]D. Kurath (private communication).